Artificial Organs

© 2018 International Center for Artificial Organs and Transplantation and Wiley Periodicals, Inc.

Fluid Dynamic Characterization of Transcatheter Aortic Valves Using Particle Image Velocimetry

*Mohammed Barakat, †Danny Dvir, and *Ali N. Azadani

*Department of Mechanical and Materials Engineering, University of Denver, Denver, CO; and †Department of Medicine, Division of Cardiology, University of Washington, Seattle, WA, USA

Abstract: Transcatheter aortic valves provide superior systolic hemodynamic performance in terms of valvular pressure gradient and effective orifice area compared with equivalent size surgical bioprostheses. However, in depth investigation of the flow field structures is of interest to examine the flow field characteristics and provide experimental evidence necessary for validation of computational models. The goal of this study was to compare flow field characteristics of the three most commonly used transcatheter and surgical valves using phase-locked particle image velocimetry (PIV). 26-mm Edwards SAPIEN 3, 26-mm Medtronic CoreValve, and 25-mm Carpentier-Edwards PERIMOUNT Magna were examined in a pulse duplicator with input parameters matching ISO-5840, that is, heart rate of 70 beats/min, cardiac output of 5 L/min, and mean aortic pressure of 100 mm Hg. A 2D PIV system was used to obtain flow velocity and viscous shear stress fields during the entire cardiac cycle. In vitro testing showed that the mean transvalvular pressure gradient was lowest for SAPIEN 3, followed by CoreValve, and PERIMOUNT Magna surgical bioprosthesis. In addition, the viscous shear stress magnitude within the jet boundary layer was higher in PERIMOUNT Magna than CoreValve and SAPIEN 3 at the peak of the flow. However, the measured shear stress values were below the known threshold for platelet activation and red blood damage. Therefore, shear-induced platelet activation is unlikely to take place during systole in the three bioprosthetic heart valves. The PIV measurements can be used for verification and validation of computational simulations. **Key Words:** Transcatheter aortic valve replacement—Surgical aortic valve replacement—Particle image velocimetry—Fluid dynamics—Bioprosthetic heart valve—Shear stress.

Aortic stenosis due to degenerative calcific aortic valvular disease is the main indication for aortic valve replacement in developed countries (1). In developing countries, conversely, rheumatic disease is a common cause of valvular heart disease (2,3). Each year, more than 67 500 surgical aortic valve replacements (SAVRs) are performed in the United States, and over 275 000 are done worldwide (4–6). The number patient with aortic valve disease is expected to triple by 2050 due to aging populations and high incidence of rheumatic heart disease in developing countries (7–10). Traditionally, the risks of lifelong anticoagulation therapy after surgical implantation of mechanical heart valves were evaluated against the risks of bioprosthetic valve structural deterioration and possible reoperation. Due to the promising improvements in the long-term durability of surgical bioprostheses, bioprosthetic heart valves have been recently implanted in more than 90% of patients who are over sixty years old to avoid lifelong anticoagulation treatment (11,12). In addition to SAVR, transcatheter aortic valve replacement (TAVR) has emerged as a safe and effective alternative treatment option for patients with severe symptomatic aortic stenosis deemed at high and intermediate risk for SAVR (13–15). The possibility of redo transcatheter

doi: 10.1111/aor.13290

Received December 2017; revised March 2018; accepted May 2018.

Address correspondence and reprint requests to Ali N. Azadani, PhD, The DU Cardiovascular Biomechanics Laboratory, Department of Mechanical and Materials Engineering, 2155 E. Wesley Ave, Room 439, Denver, CO 80208, USA. E-mail: ali.azadani@du.edu

Presented in part at the 70th Meeting of the American Physical Society Division of Fluid Dynamics held November 19–21, 2017 in Denver, CO, USA.

valve-in-valve implantation has also contributed to the shift toward the use of bioprostheses in patients (16–18). Consequently, the majority of patients who undergo aortic valve replacement currently receive either surgical or transcatheter bioprosthetic heart valves (12,19–21).

Unlike surgical stented bioprosthetic heart valves where leaflets are sutured to a frame mounted on a sewing ring,TAV leaflets are attached to a stent which can be expanded within the annulus. The lack of a sewing ring in TAVs can lead to a larger valve area compared to surgical bioprostheses following full expansion of the TAV stent to its nominal size. As a result, clinical measurements of transvalvular pressure gradients and effective orifice area have been shown that TAVs match and may even exceed the systolic hemodynamic function of surgical stented bioprostheses (22–24). Although, in-depth investigation of the flow field structures in TAVs using quantitative measurement techniques such as particle image velocimetry is of interest to examine the flow-field characteristics (25,26). In addition, the experimental data provide evidence necessary for verification and validation of computational models of bioprosthetic heart valves. Computational modeling and simulations are becoming increasingly accepted component in design and verification of medical devices in the past few years (27). Therefore, the goal of the study was to determine flow field characteristics of the two commercially available TAV devices, Edwards SAPIEN 3, and Medtronic CoreValve, during systole and compare it with that of a commonly used surgical bioprosthesis, Carpentier-Edwards PERIMOUNT Magna valve, using phase-locked particle image velocimetry (PIV) measurements.

MATERIALS AND METHODS

Edwards SAPIEN Transcatheter Heart Valve (Edwards Lifesciences) and Medtronic CoreValve (Medtronic, Minneapolis, MN, USA) have been widely used in clinical trials and clinical practice. Edwards SAPIEN valve consists of a balloon-expandable stent and bovine pericardial leaflets. Conversely, Medtronic CoreValve is constructed from a self-expanding nitinol stent and porcine pericardial leaflets. Both devices were granted CE Mark approval for commercial use in Europe in 2007. In addition, the U.S. Food and Drug Administration approved the indication for the systems to include treatment of patients with severe aortic stenosis at high and intermediate risk for surgery. In this study, detailed flow-field characteristics of 26-mm Edwards SAPIEN 3 and 26-mm Medtronic CoreValve were determined and compared with that of a 25-mm surgical Carpentier-Edwards PERIMOUNT Magna aortic heart valve (Edwards Lifesciences Fig. 1).

A custom-built pulse duplicator system (BDC Labs, Wheat Ridge, CO, USA) was used for testing the three bioprosthetic heart valves (Fig. 2). Heart rate and cardiac output were control parameters for a virtual LabVIEW pulse-signal-generator that controls a servo pump system. Each stroke of the pump's piston changes the pressure surrounding a compliant silicone ventricle, causing ejection through the aortic valve. Custom-made silicone washers (outer diameter 40 mm, inner diameter labeled size of the bioprostheses, and thickness 10 mm) were employed to mount the bioprosthetic valves. The Carpentier-Edwards PERIMOUNT Magna bioprosthesis was placed on the top of the silicone washer and sutures

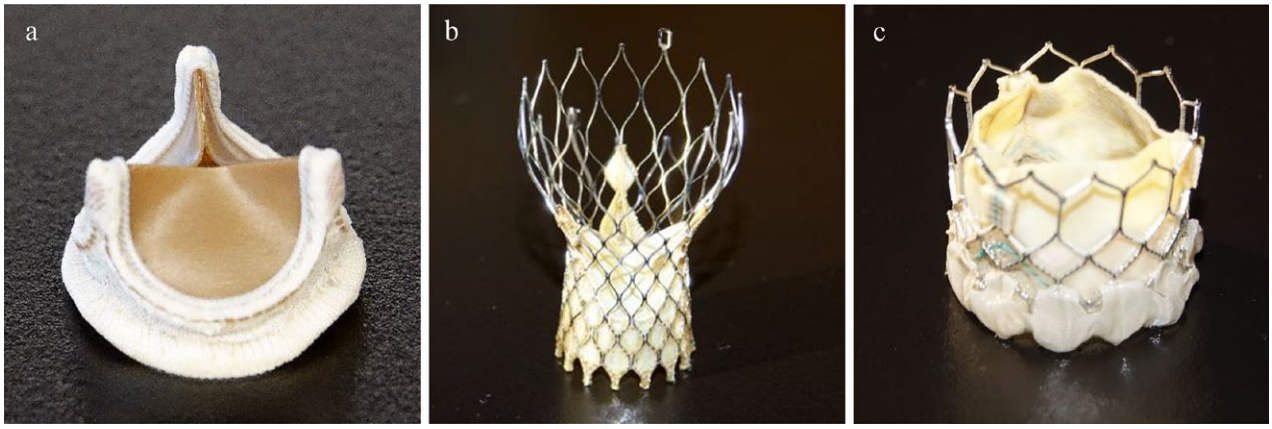

FIG. 1. (a) 25-mm surgical Carpentier-Edwards PERIMOUNT Magna bioprosthetic aortic valve. (b) 26-mm self-expanding Medtronic CoreValve. (c) 26-mm Edward SAPIEN 3 transcatheter heart valve.

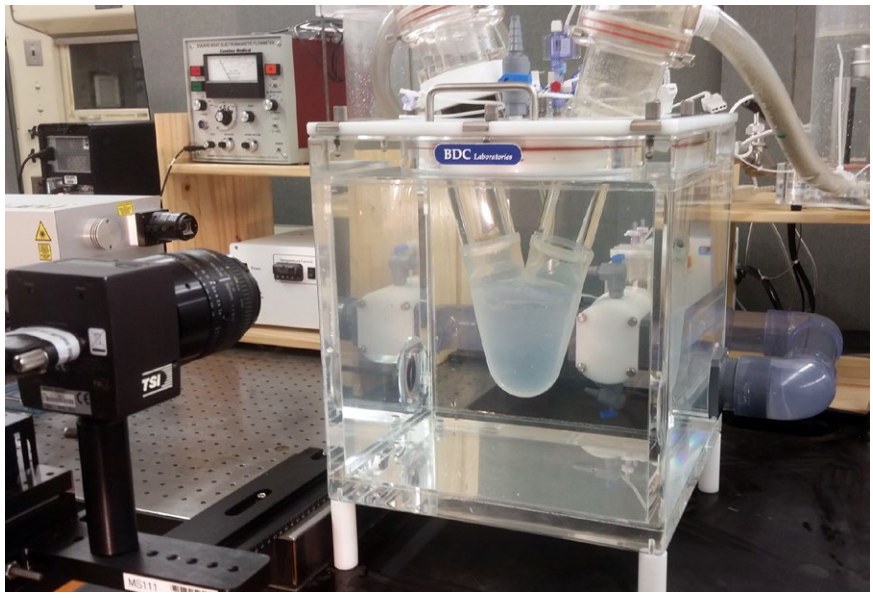

FIG. 2. Custom-built pulse duplicator system and PIV setup.

were passed through the sewing ring to hold the valve in place. In addition, the two TAVs were placed within the custom-made silicone washers, so that the bottom of the TAV frame (stent) was at the same level as the bottom of the silicone washer. A bileaflet mechanical heart valve was placed on the other side of the silicone ventricle in the mitral valve position. The pulse duplicator input parameters matched the international standard ISO 5840: 2015 recommendations for testing prosthetic heart valves; that is, heart rate of 70 beats/min, mean atrial and aortic pressures of 10 and 100 mm Hg, and cardiac output of 5 L/min. The physiological flow condition was simulated by controlling peripheral resistance in the pulse duplicator and local compliance using two compliance chambers downstream of the aortic valve. Recirculating fluid of 45% by volume glycerin solution (99% The Science Company, Denver, CO, USA) in phosphate buffered normal saline solution (Research Products International, Mount Prospect, IL, USA) was used as a blood analog fluid. The running solution has a viscosity of 3.45 cP, a density of 1.12 g/cm^3, and a refractive index of 1.39 at 37°C. Pressure was measured in the aorta and left ventricle using strain gauge pressure transducers (Utah Medical Products, Midvale, UT, USA) embedded inside the pulse duplicator 35 mm upstream and 105 mm downstream of the bioprostheses. The pressure transducers were calibrated prior to the tests using Delta-Cal Pressure transducer simulator/tester (Utah Medical Products, Inc). In addition, an electromagnetic flowmeter (Model 501, Carolina Medical Electronics Inc, East Bend, NC, USA) was used to measure flow rate in the system. Moreover, motion of the leaflets was captured using a high-speed camera (Sony DSC-RX10M3) placed on top of the aortic valve at rates of 480 and 960 frames per second.

A conventional two-dimensional PIV system (TSI, Inc., Shoreview, MN, USA) was used to obtain planar velocity measurements downstream of the bioprosthetic valves. Illumination was supplied by a dual oscillator Nd:YAG laser (Litron Lasers Nano S 15 Hz) and lasers were synchronized using a Laser Pulse Synchronizer (TSI, model 610035, TSI Inc.). Silver coated hollow glass particles (8 μm diameter, TSI, model 10089-SLVR) were used to visualize the flow. Images were recorded with a 1600 × 1200-pixel resolution crosscorrelation CCD camera (Power View Plus 2MP, TSI, model 630157), capable of capturing PIV image pairs at 30 frames per second. For PIV measurement, the camera was fitted to a NIKKOR lens (50 mm f/1.8D) and a narrow band interference filter was utilized to reduce reflections. The spatial resolution for the Magna surgical bioprosthesis, CoreValve, and SAPIEN 3 was 58.96 μm/pixel, 62.29 μm/pixel, and 56.29 μm/pixel, respectively. Phase-locked measurements were acquired by triggering the PIV system from the pulse generator driving the piston pump, over 91-time instances regularly spaced over the entire cardiac cycle. All images were correlated on a recursive Nyquist grid using a 50% overlap with a final pass interrogation window of 24 × 24 pixels. The final interrogation size was selected to have a careful balance between the highest resolution and the signal-to-noise ratio of the cross correlations. Data was processed using INSIGHT

3G TM software from TSI. For simple nondeforming solid boundaries, such as straight pipes, calibration codes can be applied to the PIV measurements to remove the optical distortion caused by the refractive index mismatch between the working fluid and the valve-mounting chamber. For calibration, a plate with a regular pattern of markers was placed in the field of view along the bioprosthetic centerline. The image was then used to define the scale and determine the image distortion in both radial and axial directions. Subsequently, a correction function was determined and a calibration MATLAB code was applied to the PIV measurements to remove the optical distortion caused by the mismatch of the refractive index of the working fluid and that of the straight cylindrical pipe (28). After obtaining the velocity field, Tecplot software (Tecplot Inc., Bellevue, WA, USA) was adopted to obtain instantaneous viscous shear stress from the measured 2D velocity gradient using Newton's law of viscosity.

RESULTS

The raw pressure and flow waveforms obtained from the three bioprosthetic heart valves in the pulse duplicator are shown in Fig. 3. The 25-mm Carpentier-Edwards PERIMOUNT Magna bioprosthesis had a mean pressure gradient of 8.6 ± 0.07 mm Hg (Fig. 3a).

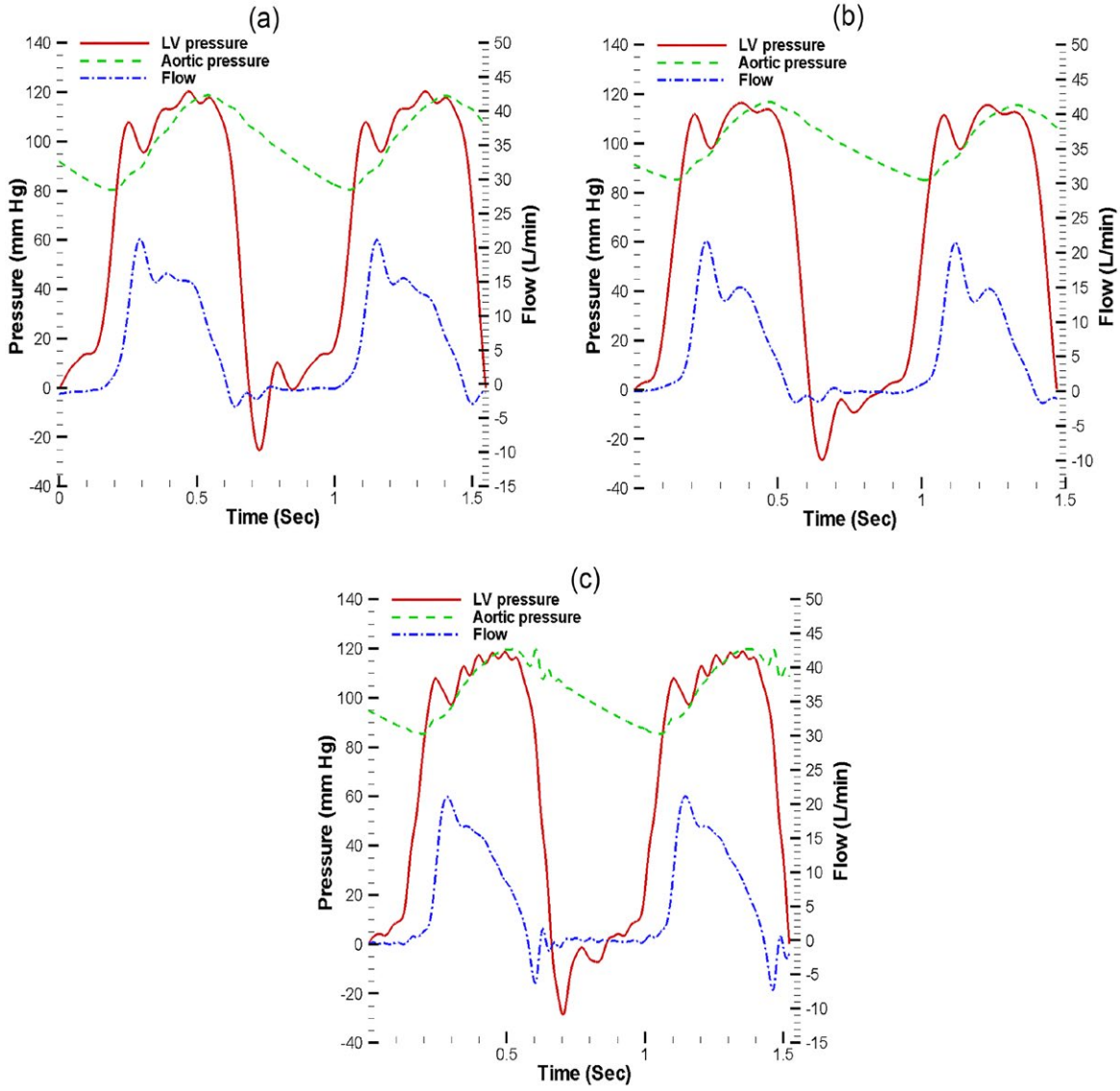

FIG. 3. In vitro pressure and flow waveforms of (a) 25-mm surgical Carpentier-Edwards PERIMOUNT Magna bioprosthetic aortic valve, (b) 26-mm self-expanding Medtronic CoreValve, and (c) 26-mm Edward SAPIEN 3 transcatheter heart valve.

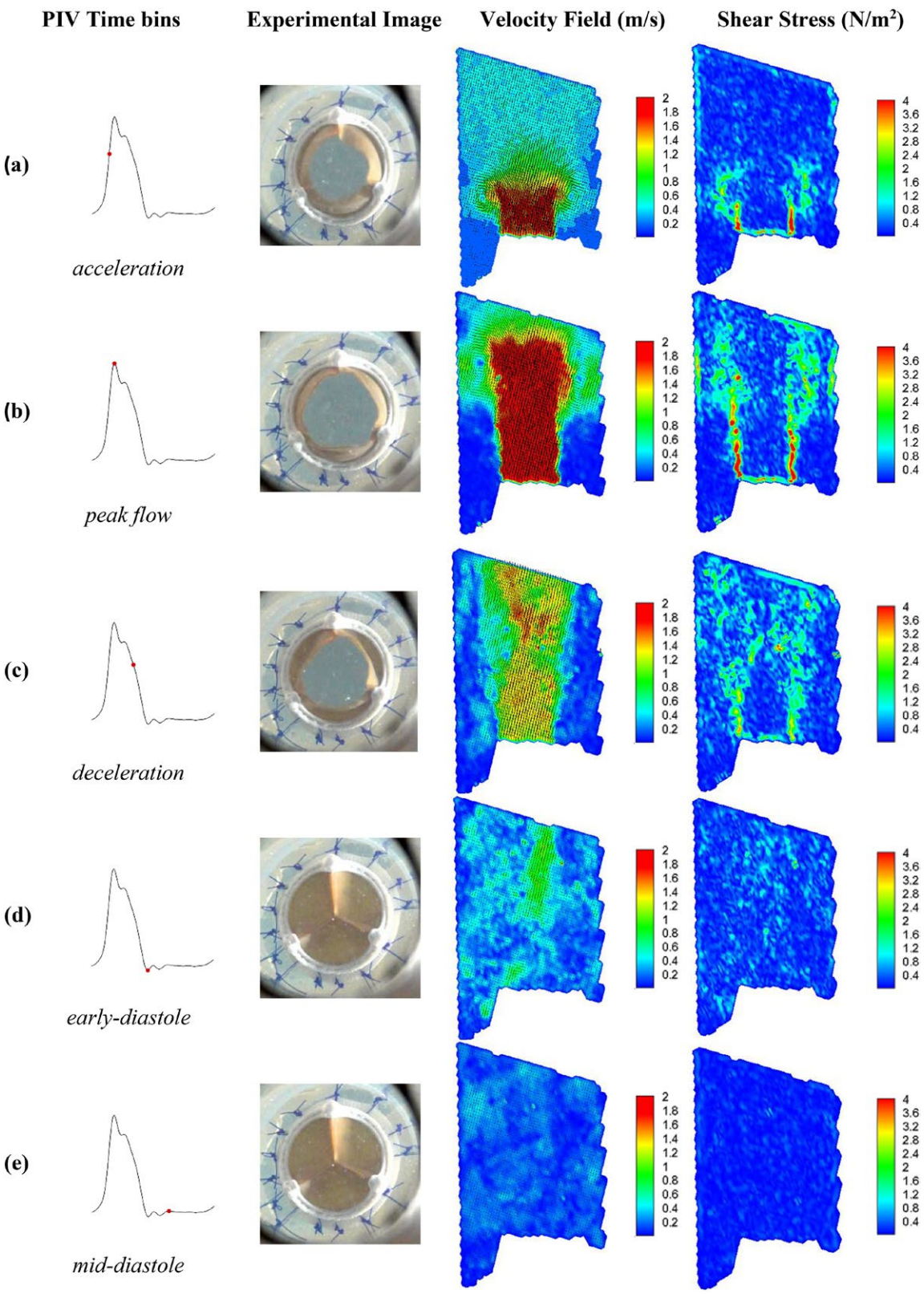

FIG. 4. Instantaneous velocity and viscous shear stress fields of 25-mm surgical Carpentier-Edwards PERIMOUNT Magna bioprosthesis in various phases of a cardiac cycle.

In addition, the effective orifice area of the bioprosthesis was 1.7 ± 0.03 cm^2. The effective orifice area was calculated based on the Gorlin equation. The 26-mm CoreValve, conversely, had a mean pressure gradient of 7.5 ± 0.16 mm Hg and an effective orifice area of 1.72 ± 0.03 cm^2 (Fig. 3b). In addition, the 26-mm SAPIEN 3 had a mean pressure gradient of 6.2 ± 0.052 mm Hg (Fig. 3c). The effective orifice area of the Edwards SAPIEN 3 bioprosthesis was 2.0 ± 0.06 cm^2. Moreover, leaflet motion of the three bioprosthetic heart valves captured by the high-speed camera is shown in the Supporting Information videos.

Instantaneous velocity vectors and viscous shear stress values of the 25-mm Carpentier-Edwards PERIMOUNT Magna bioprosthesis are presented in Fig. 4. The time intervals presented in the figure correspond to five different phases within a cardiac cycle, namely, acceleration, peak flow, deceleration, early-diastole, and mid-diastole. In the acceleration phase, a highly axial flow velocity was observed along the bioprosthetic centerline (Fig. 4a). At the peak of flow, a maximum jet velocity of 2.1 m/s was measured in the center of the jet (Fig. 4b). The jet diameter at the peak of flow was approximately 15.2 mm. The velocity decreased abruptly from the strong central jet to the surrounding region. During deceleration phase, velocity of the jet at the core was decreased to 1.2 m/s (Fig. 4c). Furthermore, significantly lower velocity magnitudes were observed after the valve closure both in early- and mid-diastole (Fig. 4d,e). In addition to the velocity field, Fig. 4 demonstrates viscous shear stress fields throughout one cardiac cycle. At the peak of the flow, maximum viscous shear stress was 4 N/m^2 and occurred along a significant portion of the jet boundary layer (Fig. 4b). During deceleration phase and in the diastole, however, viscous shear stress was significantly lower than the magnitudes observed at the peak of the flow (Fig. 4c–e).

Velocity and viscous shear stress fields of the 26-mm Medtronic CoreValve are presented in Fig. 5. During the acceleration phase, as presented in Fig. 5a, PIV measurements showed an accelerating axial flow along the valve centerline. At peak of the systole, a maximum velocity of 2.2 m/s was measured in the center of the jet (Fig. 5b). The diameter of the jet velocity was approximately 11.3 mm, which was smaller than that of the PERIMOUNT Magna bioprosthesis. During the deceleration phase, velocity magnitude considerably dropped as shown in Fig. 5c. In addition, even lower velocity magnitudes were observed during the diastole after the valve closure (Fig. 5d,e). In addition to the velocity field, Fig. 5 illustrates viscous shear stress magnitude throughout the five phases of one cardiac cycle. At the peak of flow, maximum viscous shear stress was 4 N/m^2 (Fig. 5b). However, due to the relatively wider jet boundary layer in CoreValve compared to the PERIMOUNT Magna valve, the overall magnitude of the viscous shear stress at the peak of flow was lower in the CoreValve than the PERIMOUNT Magna bioprosthesis. During the deceleration phase and during diastole, the maximum viscous shear stress magnitude was significantly lower than the peak of the flow as presented in Fig. 5c–e. Local pockets of elevated viscous shear stress were found within the flow field downstream of the bioprosthesis.

In addition, Fig. 6 shows instantaneous velocity vectors and viscous shear stress field of the 26-mm Edwards SAPIEN 3 bioprosthesis. The first image row shows the acceleration phase, in which an accelerating axial flow can be clearly observed along the bioprosthetic centerline (Fig. 6a). After 40 ms, at the peak of flow, a strong jet with a maximum velocity of 1.9 m/s was observed (Fig. 6b). The jet diameter was approximately 20.9 mm, which was more than the Medtronic CoreValve and PERIMOUNT Magna bioprosthesis. During the deceleration phase, as shown in Fig. 6c, velocity of the central jet decreased to 1.3 m/s. Furthermore, significantly lower velocity magnitudes were observed in the early- and mid-diastole following the closure of the bioprosthesis (Fig. 6d,e). In addition, Fig. 6 shows viscous shear stress magnitudes that were obtained from the velocity field throughout one cardiac cycle. In the peak flow, maximum viscous shear stress was 4 N/m^2 and occurred at the jet boundary layer (Fig. 6b). However, the overall magnitude of the viscous shear stress at the peak of flow within the jet boundary layer was lower in the SAPIEN 3 than the PERIMOUNT Magna bioprosthesis. In addition, during deceleration phase and during diastole, the maximum viscous shear stress was significantly lower than the magnitudes observed at the peak of the flow (Fig. 6c–e).

DISCUSSION

In this study, we determined flow field characteristics of the two commercially available and commonly used TAVs, Edwards SAPIEN 3, and Medtronic CoreValve, using phase-locked PIV measurements and compared the results with that of a commonly used surgical bioprosthesis, Carpentier-Edwards PERIMOUNT Magna bioprosthesis. The overall systolic hemodynamic performance of the

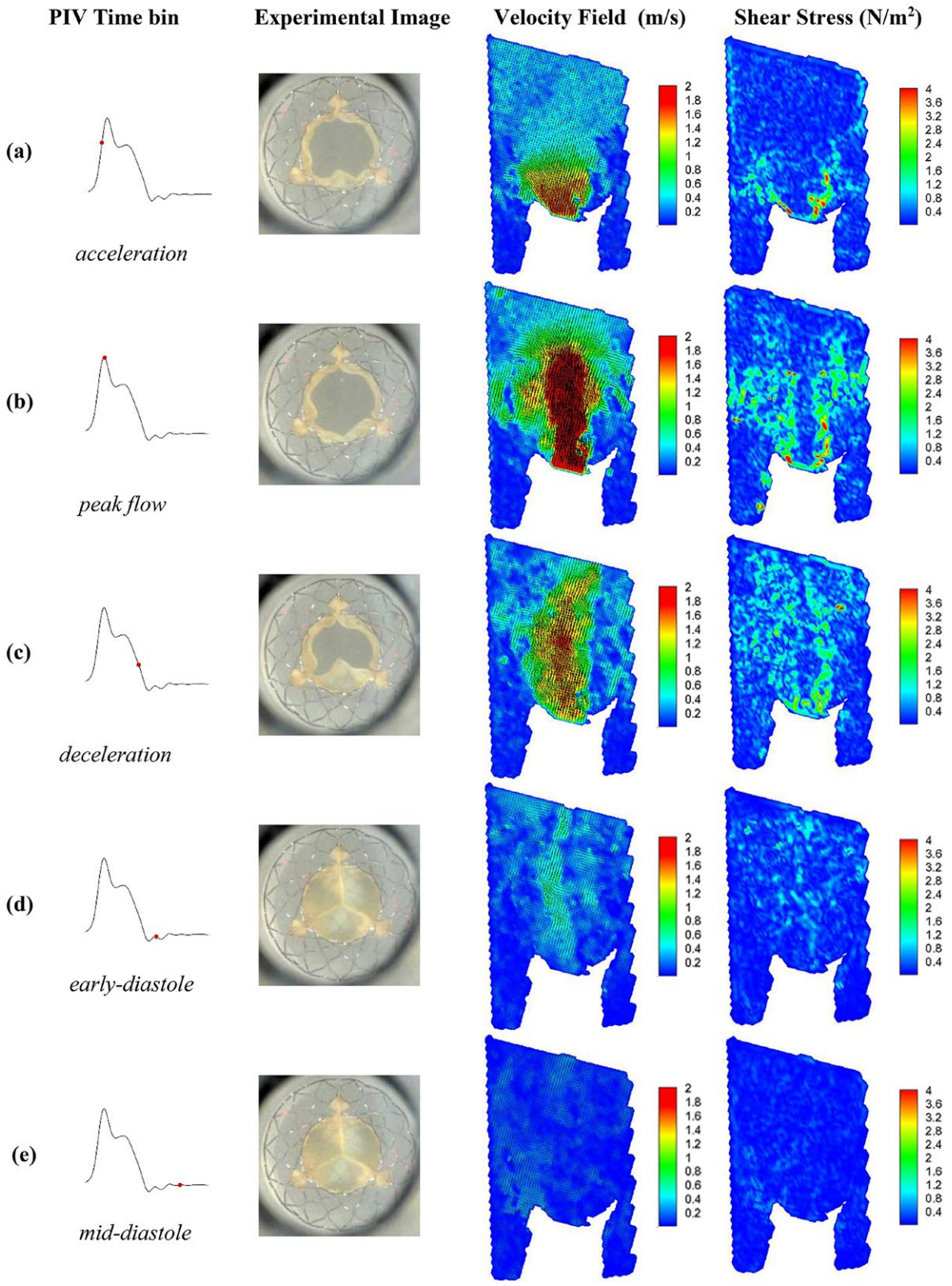

FIG. 5. Instantaneous velocity and viscous shear stress fields of 26-mm Medtronic CoreValve in various phases of a cardiac cycle.

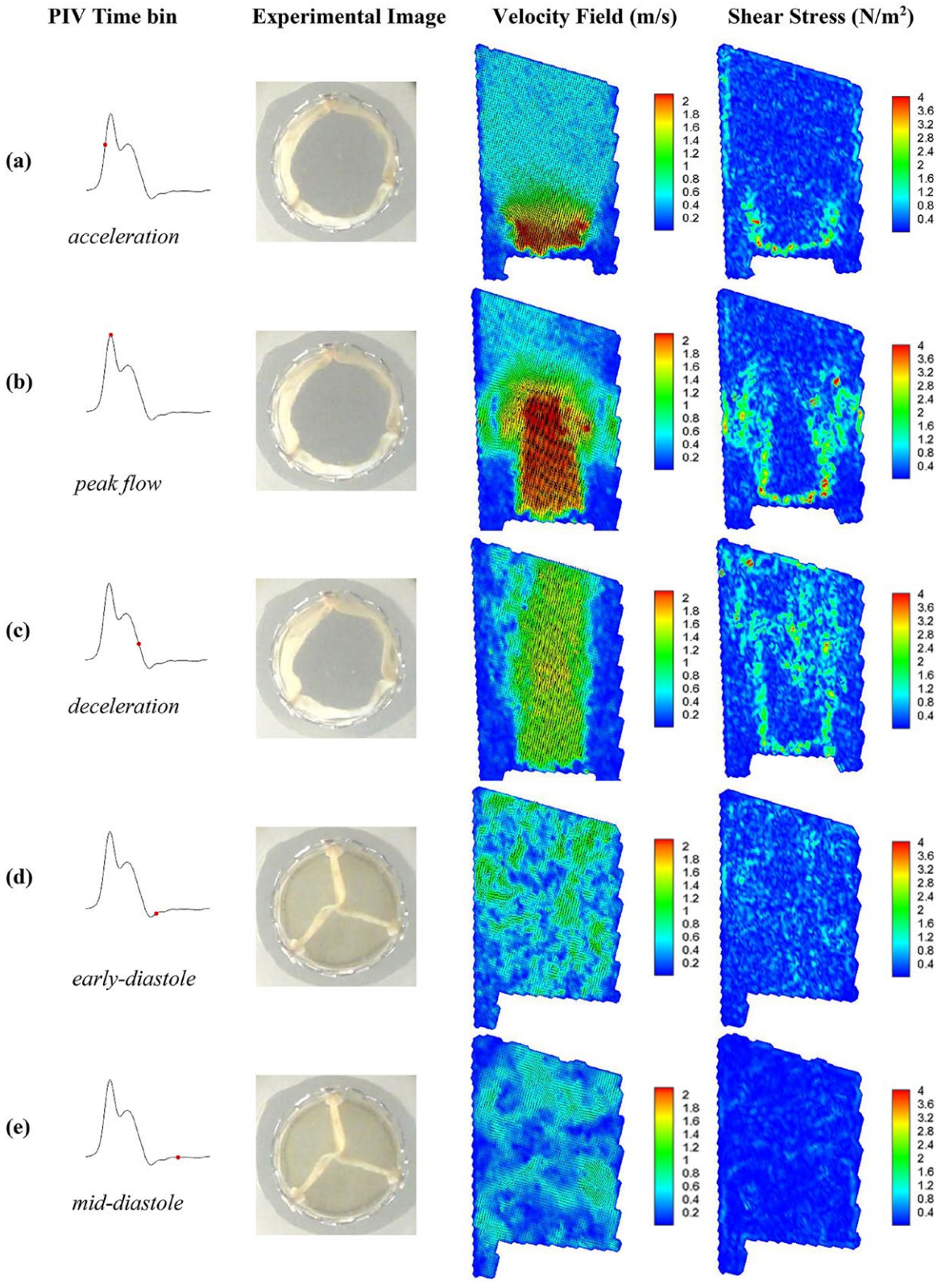

FIG. 6. Instantaneous velocity and viscous shear stress fields of 26-mm Edwards SAPIEN 3 in various phases of a cardiac cycle.

26-mm Medtronic CoreValve and 26-mm Edwards SAPIEN 3, in terms of the mean transvalvular pressure gradient and effective orifice area, was slightly superior to that of the 25-mm Carpentier-Edwards PERIMOUNT Magna bioprosthesis. The observation was consistent with the clinical hemodynamic measurements of the bioprostheses (29,30). Due to the lack of sewing ring in TAVs, TAV devices offer a larger orifice area than comparabled size surgical bioprostheses after full expansion of the TAV stent to its nominal size. In addition, the maximum viscous shear stress magnitude within the jet boundary layer at the peak of the flow was higher in PERIMOUNT Magna than CoreValve and SAPIEN 3 bioprostheses. In addition, the velocity jet diameter was relatively narrower in the Medtronic CoreValve than SAPIEN 3 and PERIMOUNT Magna, which was due to the conical inflow section of the CoreValve. The velocity measurements were comparable with majority of previous studies using 2D PIV to obtain velocity profiles of surgical bioprosthetic valves (31,32).

Fluid dynamics has been known to play a critical role in thrombotic and hemolytic complications associated with prosthetic heart valves (26,33). Thromboembolic events due to hemolysis and shear-induced platelet activation have been correlated to high shear stress regions in the blood flow (34–36). The true shear force experienced by blood cells is caused by viscous shear stress than Reynolds shear stress in the presence of turbulence (37,38). It is well known that both shear stress magnitude and exposure time are important in activation of blood cell elements. The higher the exposure time, the lower would be the stress threshold level for blood cell impairment. The shear stress magnitude of 150 N/m^2 is known to be the threshold under which no red blood cell damage has been observed regardless of the exposure time (39). In the current study, the measured viscous shear stress downstream of the three bioprostheses was significantly below the threshold level for red blood cell damage reported in the literature. Conversely, shear-induced platelet activation occurs at significantly lower shear stress values. Hung et al. (40) reported platelet damage at 10–16.5 N/m^2 for an exposure time of 10^2 s, while Williams (41) found a threshold of 13 N/m^2 for exposure time levels of 10^{-3} s. In addition, Ramstack et al. (42) reported platelet activation at a somewhat higher threshold of 30–100 N/m^2 with an exposure time of 10^{-2}–10^1 s. The measured shear stress values in the three bioprosthetic heart valves examined in this study were significantly below platelet activation threshold reported in the literature. As a result, the predominant mechanism of platelet activation in the bioprosthetic heart valves will likely be as a result of blood contact with foreign surfaces of bioprostheses than shear-induced platelet activation.

In vitro experimental testing has been an integral part of design verification and optimization of medical devices. In the past few years, the role of computational modeling and simulations in design and verification of prosthetic heart valves is becoming more and more important (43). The U.S. Food and Drug Administration (FDA) and EU Medical Device Regulatory System are major driving forces behind the trend (44,45). As a result, in vitro experimental testing such as the one presented in this study can be used to validate and verify the computational simulations (46–49). A combined experimental and computational approach should be considered to shed light on the flow-mediated mechanisms of thrombosis in bioprosthetic aortic valves. For instance, regions of blood stagnation provide an opportunity for platelets and blood proteins to accumulate to critical concentrations leading to thrombosis (50–57). Contrary to SAVR where native calcified leaflets are removed from the annulus during open heart surgery, TAVs are implanted within native valves in TAVR procedures. As a result, the aortic portion of the TAV stent is circumferentially surrounded by the calcified native valves in TAVR. This configuration is more pronounced in TAVs that tend to operate inside the annulus such as SAPIEN valves compared to supra-annular TAVs such as CoreValve. The geometric confinement of TAVs disturbs the natural flow field between the leaflets and aortic sinuses, increases the blood residence time (stasis) on the leaflets, and consequently increases the likelihood of thrombogenesis on the TAV leaflets (58–62). Remarkably, leaflet thrombosis is more commonly observed in TAVR than SAVR (11). In addition, the majority of the reported cases of leaflet thrombosis occurred after using TAVs with intra-annular design, such as Edwards SAPIEN and St. Jude Portico valves (63–65).

Study limitations

In this study, a conventional 2D PIV system was used to obtain planar velocity measurements downstream of the three bioprosthetic heart valves. In 2D PIV measurements, the third component of velocity vector cannot be measured. However, since the axial jet velocity is of such great magnitude during the systole, the third component of the velocity vector is insignificant. Therefore, the 2D PIV measurements accurately approximate the total viscous shear stress

values in the jet boundary layer during the systole. In the diastole, however, flow is three-dimensional, rotational, and spatially inhomogeneous. Therefore, other PIV methods, such as stereo-PIV and tomographic-PIV, should be utilized to measure the three components of velocity vectors. Another limitation of this study was the lack of aortic sinus and coronary flow in the pulse duplicator system. However, we believe that the limitations of the currently available in vitro experimental setups that attempt to model the aortic root geometry justify the use of the simplified geometry of the present work. For instance, in the currently available pulse duplicator systems, the aortic root does not represent a patient specific geometry, the root compliance and coronary arteries are nonexistent, and in the cases that include these properties, the resistance of coronary arteries cannot be accurately adjusted. As a result, using a simplified geometry facilitates the validation process of computational works during systole which was one of the main objectives of this study.

CONCLUSION

A comprehensive evaluation of velocity and viscous shear stress fields downstream of three commonly used bioprosthetic heart valves was performed using 2D particle image velocimetry measurements. The in vitro experiments showed that hemodynamic characteristics of the 26-mm SAPIEN 3 and 26-mm CoreValve were comparable to the 25-mm PERIMOUNT Magna surgical bioprosthesis. Maximum viscous shear stress was observed at the peak of flow during the systole within the jet boundary layer in all the three bioprostheses. The measured shear stress values were below the known threshold for red blood damage and platelet activation. Therefore, shear-induced damage to red blood cells and platelet activation are unlikely to take place during systole in all the three bioprosthesis. Despite the limitations described previously, PIV measurements can also be used for verification and validation of computational simulations.

Acknowledgment: This work was supported by graduate scholarship from Jazan University and partially by the American Heart Association Scientist Development Grant (grant number AHA16SDG309 20009).

Author Contributions: Mohammed Barakat contributed to collection of data, analysis and interpretation of data, and writing the manuscript. Danny Dvir contributed to study design and critical review of the manuscript. Ali N. Azadani contributed to study design, development of methodology, collection of data, interpretation of data, and writing the manuscript.

Conflict of Interest: Dr. Azadani reports a financial relationship as co-founder of ReValve Medical Inc. In addition, Dr. Dvir reports consulting fees from Edwards Lifesciences, Medtronic, and St. Jude.

REFERENCES

1. Iung B, Baron G, Butchart EG, et al. A prospective survey of patients with valvular heart disease in Europe: the Euro Heart Survey on Valvular Heart Disease. *Eur Heart J* 2003;24:1231–43.
2. World Health Organization. *Rheumatic Fever and Rheumatic Heart Disease: Report of a WHO Expert Consultation*. World Health Organization (WHO); Geneva, Switzerland, 20 October–1 November 2001, 2004.
3. Sliwa K, Carrington M, Mayosi BM, Zigiriadis E, Mvungi R, Stewart S. Incidence and characteristics of newly diagnosed rheumatic heart disease in urban African adults: insights from the heart of Soweto study. *Eur Heart J* 2010;31:719–27.
4. Aikawa E. Calcific Aortic Valve Disease. London, UK: IntechOpen, 2013. https://doi.org/10.5772/46239.
5. Clark MA, Duhay FG, Thompson AK, et al. Clinical and economic outcomes after surgical aortic valve replacement in Medicare patients. *Risk Manag Healthc Policy* 2012;5:117–26.
6. Rosamond W, Flegal K, Furie K, et al. Heart disease and stroke statistics—2008 update. *Circulation* 2008;117:e25–146.
7. Takkenberg JJ, Rajamannan NM, Rosenhek R, et al. The need for a global perspective on heart valve disease epidemiology. The SHVD working group on epidemiology of heart valve disease founding statement. *J Heart Valve Dis* 2008;17:135–9.
8. Yacoub M, Takkenberg J. Will heart valve tissue engineering change the world? *Nat Clin Pract Cardiovasc Med* 2005;2:60–1.
9. Nkomo VT, Gardin JM, Skelton TN, Gottdiener JS, Scott CG, Enriquez-Sarano M. Burden of valvular heart diseases: a population-based study. *Lancet* 2006;368:1005–11.
10. De Santo LS, Romano G, Della Corte A, et al. Mechanical aortic valve replacement in young women planning on pregnancy. *J Am Coll Cardiol* 2012;59:1110–5.
11. Mack M, Holmes D. Bioprosthetic valve thrombosis: the harder one looks, the more one finds. *J Thorac Cardiovasc Surg* 2016;152:952–3.
12. Isaacs AJ, Shuhaiber J, Salemi A, Isom OW, Sedrakyan A. National trends in utilization and in-hospital outcomes of mechanical versus bioprosthetic aortic valve replacements. *J Thorac Cardiovasc Surg* 2015;149:1262–9. e3.
13. Adams DH, Popma JJ, Reardon MJ, et al. Transcatheter aortic-valve replacement with a self-expanding prosthesis. *N Engl J Med* 2014;370:1790–8.
14. Smith CR, Leon MB, Mack MJ, et al. Transcatheter versus surgical aortic-valve replacement in high-risk patients. *N Engl J Med* 2011;364:2187–98.
15. Leon MB, Smith CR, Mack MJ, et al. Transcatheter or surgical aortic-valve replacement in intermediate-risk patients. *N Engl J Med* 2016;374:1609–20.
16. Dvir D, Webb JG, Bleiziffer S, et al. Transcatheter aortic valve implantation in failed bioprosthetic surgical valves. *JAMA* 2014;312:162–70.

17. Azadani AN, Tseng EE. Transcatheter heart valves for failing bioprostheses. *Circ Cardiovasc Interv* 2011;4:621–8.
18. Azadani AN, Tseng EE. Transcatheter valve-in-valve implantation for failing bioprosthetic valves. *Future Cardiol* 2010;6:811–31.
19. Lund O, Bland M. Risk-corrected impact of mechanical versus bioprosthetic valves on long-term mortality after aortic valve replacement. *J Thorac Cardiovasc Surg* 2006;132:20–6. e3.
20. Puvimanasinghe J, Takkenberg J, Edwards M, et al. Comparison of outcomes after aortic valve replacement with a mechanical valve or a bioprosthesis using microsimulation. *Heart* 2004;90:1172–8.
21. Sun JC, Davidson MJ, Lamy A, Eikelboom JW. Antithrombotic management of patients with prosthetic heart valves: current evidence and future trends. *Lancet* 2009;374:565–76.
22. Daubert MA, Weissman NJ, Hahn RT, et al. Long-term valve performance of TAVR and SAVR: a report from the PARTNER I trial. *JACC Cardiovasc Imaging* 2017;10:15–25.
23. Hahn RT, Pibarot P, Stewart WJ, et al. Comparison of transcatheter and surgical aortic valve replacement in severe aortic stenosis. *J Am Coll Cardiol* 2013;61:2514–21.
24. Clavel M-A, Webb JG, Pibarot P, et al. Comparison of the hemodynamic performance of percutaneous and surgical bioprostheses for the treatment of severe aortic stenosis. *J Am Coll Cardiol* 2009;53:1883–91.
25. Stühle S, Wendt D, Hou G, et al. In-vitro investigation of the hemodynamics of the Edwards Sapien™ transcatheter heart valve. *J Heart Valve Dis* 2011;20:53.
26. Dasi LP, Simon HA, Sucosky P, Yoganathan AP. Fluid mechanics of artificial heart valves. *Clin Exp Pharmacol Physiol* 2009;36:225–37.
27. Stewart SF, Hariharan P, Paterson EG, et al. Results of FDA's first interlaboratory computational study of a nozzle with a sudden contraction and conical diffuser. *Cardiovasc Eng Technol* 2013;4:374–91.
28. Vahidkhah K, Barakat M, Abbasi M, et al. Valve thrombosis following transcatheter aortic valve replacement: significance of blood stasis on the leaflets. *Eur J Cardiothorac Surg* 2017;51:927–35.
29. Külling M, Külling J, Wyss C, et al. Effective orifice area and hemodynamic performance of the transcatheter Edwards Sapien 3 prosthesis: short-term and 1-year follow-up. *Eur Heart J Cardiovasc Imaging* 2018;19:23–30.
30. Spethmann S, Dreger H, Schattke S, et al. Doppler haemodynamics and effective orifice areas of Edwards SAPIEN and CoreValve transcatheter aortic valves. *Eur Heart J Cardiovasc Imaging* 2012;13:690–6.
31. Raghav V, Okafor I, Quach M, Dang L, Marquez S, Yoganathan AP. Long-term durability of Carpentier-Edwards Magna Ease valve: a one billion cycle in vitro study. *Ann Thorac Surg* 2016;101:1759–65.
32. Moore BL, Dasi LP. Coronary flow impacts aortic leaflet mechanics and aortic sinus hemodynamics. *Ann Biomed Eng* 2015;43:2231–41.
33. Yoganathan AP, He Z, Casey Jones S. Fluid mechanics of heart valves. *Annu Rev Biomed Eng* 2004;6:331–62.
34. Becker RC, Eisenberg P, Turpie AG. Pathobiologic features and prevention of thrombotic complications associated with prosthetic heart valves: fundamental principles and the contribution of platelets and thrombin. *Am Heart J* 2001;141:1025–37.
35. Vahidkhah K, Cordasco D, Abbasi M, et al. Flow-induced damage to blood cells in aortic valve stenosis. *Ann Biomed Eng* 2016;44:2724–36.
36. Alemu Y, Bluestein D. Flow-induced platelet activation and damage accumulation in a mechanical heart valve: numerical studies. *Artif Organs* 2007;31:677–88.
37. Ge L, Dasi LP, Sotiropoulos F, Yoganathan AP. Characterization of hemodynamic forces induced by mechanical heart valves: Reynolds vs. viscous stresses. *Ann Biomed Eng* 2008;36:276–97.
38. Jones SA. A relationship between Reynolds stresses and viscous dissipation: implications to red cell damage. *Ann Biomed Eng* 1995;23:21–8.
39. Leverett L, Hellums J, Alfrey C, Lynch E. Red blood cell damage by shear stress. *Biophys J* 1972;12:257–73.
40. Hung TC, Hochmuth RM, Joist JH, Sutera SP. Shear-induced aggregation and lysis of platelets. *Trans Am Soc Artif Intern Organs* 1976;22:285–91.
41. Williams AR. Release of serotonin from human platelets by acoustic microstreaming. *J Acoust Soc Am* 1974;56:1640–9.
42. Ramstack JM, Zuckerman L, Mockros LF. Shear-induced activation of platelets. *JBiomech* 1979;12:113–25.
43. Oberkampf WL, Trucano TG, Hirsch C. Verification, validation, and predictive capability in computational engineering and physics. *Appl Mech Rev* 2004;57:345–84.
44. Stewart SF, Paterson EG, Burgreen GW, et al. Assessment of CFD performance in simulations of an idealized medical device: results of FDA's first computational interlaboratory study. *Cardiovasc Eng Technol* 2012;3:139–60.
45. Morris PD, Narracott A, von Tengg-Kobligk H, et al. Computational fluid dynamics modelling in cardiovascular medicine. *Heart* 2016;102:18–28.
46. Dwyer HA, Matthews PB, Azadani A, et al. Computational fluid dynamics simulation of transcatheter aortic valve degeneration. *Interact Cardiovasc Thorac Surg* 2009;9:301–8.
47. Sirois E, Sun W. Computational evaluation of platelet activation induced by a bioprosthetic heart valve. *Artif Organs* 2011;35:157–65.
48. Hsu M-C, Kamensky D, Xu F, et al. Dynamic and fluid–structure interaction simulations of bioprosthetic heart valves using parametric design with T-splines and Fung-type material models. *Comput Mech* 2015;55:1211–25.
49. Tan F, Xu X, Torii R, et al. Comparison of aortic flow patterns before and after transcatheter aortic valve implantation. *Cardiovasc Eng Technol* 2012;3:123–35.
50. Brotman DJ, Deitcher SR, Lip GY, Matzdorff AC. Virchow's triad revisited. *South Med J* 2004;97:213–5.
51. Anning S. The historical aspects of venous thrombosis. *Med Hist* 1957;1:28–37.
52. Karino T, Goldsmith H. Aggregation of human platelets in an annular vortex distal to a tubular expansion. *Microvasc Res* 1979;17:217–37.
53. Bluestein D, Niu L, Schoephoerster RT, Dewanjee MK. Fluid mechanics of arterial stenosis: relationship to the development of mural thrombus. *Ann Biomed Eng* 1997;25:344–56.
54. Goodman PD, Barlow ET, Crapo PM, Mohammad SF, Solen KA. Computational model of device-induced thrombosis and thromboembolism. *Ann Biomed Eng* 2005;33:780–97.
55. Friedrich P, Reininger A. Occlusive thrombus formation on indwelling catheters: in vitro investigation and computational analysis. *Thromb Haemost* 1995;73:66–72.
56. Reininger AJ, Heinzmann U, Reininger CB, Friedrich P, Wurzinger LJ. Residence time in niches of stagnant flow determines fibrin clot formation in an arterial branching model–detailed flow analysis and experimental results. *Thromb Haemost* 1994;74:629–2.
57. Sukavaneshvar S. Device thrombosis and pre-clinical blood flow models for assessing antithrombogenic efficacy of drug-device combinations. *Adv Drug Deliv Rev* 2017;112:24–34.
58. Vahidkhah K, Barakat M, Abbasi M, Javani S, Azadani PN, Tandar A. Valve thrombosis following transcatheter aortic valve replacement: significance of blood stasis on the leaflets. *Eur J Cardiothorac Surg* 2017;51:927–35.

59. Vahidkhah K, Javani S, Abbasi M, et al. Blood stasis on transcatheter valve leaflets and implications for valve-in-valve leaflet thrombosis. *Ann Thorac Surg* 2017;104:751–759.
60. Vahidkhah K, Azadani AN. Supra-annular Valve-in-Valve implantation reduces blood stasis on the transcatheter aortic valve leaflets. *JBiomech* 2017;58:114–22.
61. Vahidkhah K, Abbasi M, Barakat M, et al. Effect of reduced cardiac output on blood stasis on transcatheter aortic valve leaflets: implications for valve thrombosis. *EuroIntervention* 2017;13:811–9.
62. Midha PA, Raghav V, Sharma R, et al. The fluid mechanics of transcatheter heart valve leaflet thrombosis in the neo-sinus. *Circulation* 2017;136:1598–1609.
63. Cordoba-Soriano JG, Puri R, Amat-Santos I, et al. Valve thrombosis following transcatheter aortic valve implantation: a systematic review. *Rev Esp Cardiol* 2015;68:198–204.
64. Makkar RR, Fontana G, Jilaihawi H, et al. Possible subclinical leaflet thrombosis in bioprosthetic aortic valves. *N Engl J Med* 2015;373:2015–24.
65. Leetmaa T, Hansson NC, Leipsic J, et al. Early aortic transcatheter heart valve thrombosis diagnostic value of contrast-enhanced multidetector computed tomography. *Circ Cardiovasc Interv* 2015;8:e001596.

SUPPORTING INFORMATION

Additional supporting information may be found online in the Supporting Information section at the end of the article.

Video S1. High speed video of 25-mm surgical Carpentier-Edwards PERIMOUNT Magna aortic heart valve at a rate of 480 frames per second.

Video S2. High speed video of 26-mm Medtronic CoreValve transcatheter aortic valve at a rate of 480 frames per second.

Video S3. High speed video of 26-mm Edwards SAPIEN 3 transcatheter aortic valve at a rate of 480 frames per second.